Bull. Mater. Sci. (2023)46:15
https://doi.org/10.1007/s12034-022-02852-9

Optical and structural properties of 2D transition metal dichalcogenides semiconductor MoS_2

KRISHNA GOPAL MONDAL*, PARESH CHANDRA JANA and SATYAJIT SAHA
Department of Physics, Vidyasagar University, Midnapore 721102, India
*Author for correspondence (rspt_krishnagopalm@mail.vidyasagar.ac.in)

MS received 1 July 2022; accepted 6 September 2022

Abstract. Two-dimensional molybdenum sulphide (MoS_2) has been synthesized by hydrothermal method, and for optical characteristics, absorption and photoluminescence spectra are recorded. Variation of refractive index, extinction coefficient, dielectric constant (both real and imaginary) and optical conductivity with wavelength have been plotted. The exciton energy has been calculated in the weak electron–phonon coupling regime. The temperature-dependent splitting energy of valance band is well explained by using simulation. Splitting energy is constant up to 50 K and then decreases with increase in temperature. Average lifetime (0.75 ns) of excited electrons have been calculated using time-correlated single photon counting. X-ray diffraction (XRD), Raman spectra and high-resolution transmission electron microscope (HRTEM) have been recorded to investigate structural properties of MoS_2 sample. XRD shows hexagonal crystal symmetry with well-defined crystallinity. In Raman spectra, three prominent peaks are found at 381, 407 and 453 cm^{-1}. HRTEM also confirms that the structure of MoS_2 is hexagonal with three layers of nano-sheet with inter-planner spacing of 0.58 nm

Keywords. Molybdenum sulphide; dielectric constant; splitting energy; photocatalytic activity; nano flake; exciton energy.

1. Introduction

Recently, many researchers have investigated on semiconducting nanomaterials due to their potential properties (optical, electronic, catalytic, etc.) and powerful applications in different branches, such as solar cell, photo detector, photocatalytic, energy storage, optoelectronic device, etc. [1–4]. The optical and electronic properties of semiconducting materials are dealt with the different applications. The efficiency of the activity has also been increased due to enhanced optical and electronic properties [3,5]. Among the semiconductor materials, two-dimensional transition metal dichalcogenide semiconductors (TMDCs) have tunable optical properties to make application in devices [6–8].

Layered structure transition metal dichalcogenide semiconductors has co-valent bond in-plane and weak Van der wall's force out-of-plane [9]. Due to this layered structure of TMDCs, bandgap energy and optical and electronic properties can be tuned by decreasing number of layers [10]. Among all TMDCs, MoS_2 is attractive semiconductor due to its remarkable optical, electronic and catalytic properties and has wide range of applications in different field of solar cells, gas sensor, energy storage, photocatalysis, etc. [11–14]. MoS_2 has a direct and indirect bandgap of 1.9 and 1.2 eV for mono layer and bulk materials, respectively, due to quantum confinement [15].

Different methods like mechanical exfoliation, chemical vapour deposition, hydrothermal, etc. have been investigated for synthesis of molybdenum sulphide (MoS_2). Feng *et al* [16] synthesized MoS_2 nano-flakes by rheological phase reaction method to investigate electrical properties. Wang *et al* [14] synthesized MoS_2 nanostructure for studying energy storage properties. Saha *et al* [17] prepared spherical amorphous MoS_2 by simple solvothermal decomposition for photocatalytic rose Bengal dye degradation. Luo *et al* [18] synthesized different types of morphology by hydrothermal method for photocatalytic application. In this work, MoS_2 nano-flakes have been synthesized by simple and convenient hydrothermal method to study optical and electronic properties.

Due to high demand for textile products, the use of synthetic dyes has been gradually increased and it releases large amount of dying waste, which pollutes both land and fresh water. Photocatalytic degradation is one of the convenient processes to treat waste water in a cost-effective way [19,20]. Here, photocatalytic effect of few-layered MoS_2 has been demonstrated by decomposing methylene blue (MB) dye in water solution under visible-light irradiation.

Published online: 19 January 2023

2. Experimental

2.1 *Materials*

To prepare MoS_2 nano-crystal, high-purity molybdenum trioxide (MoO_3) and potassium thiocyanate (KSCN) were purchased from Merk Life Science Private Limited. Also, sodium hydroxide (NaOH) and 35% hydrochloric acid (HCl), ethanol, methylene blue (MB) and double-distilled water were taken. All reagents were used without further purification.

2.2 *Synthesis method*

Molybdenum sulphide (MoS_2) nano-flakes have been grown using hydrothermal method. In this typical process, molybdenum trioxide (MoO_3) and potassium thiocyanate (KSCN) were used as molybdenum and sulker precursors, respectively. At first, 288 mg molybdenum trioxide and 388 mg potassium thiocyanate (1:2 molar ratio) were mixed with 40 ml double-distilled water via ultra-sonication for 60 min. To fix pH value 2.0, 1 mol l^{-1} HCl solution was compiled and then mixed solution were stirred for 15 min with the magnetic stirrer. After that, the mixed solution was shifted into a 50 ml autoclave at 230°C for 30 h. Then it was cooled down normally to room temperature and centrifuged at 5000 rpm for 10 min. Finally, the prepared sample was washed several times with double-distilled water and ethanol to remove different ions, and it was kept in a vacuum desiccator at room temperature for 2 days for drying. Prepared powder sample was heated at 40°C for 6 h to remove any moisture in it.

2.3 *Sample characterization*

For investigation of optical properties of the prepared molybdenum sulphide (MoS_2), absorption spectra were recorded from 250 to 800 nm by using Carry 5000 UV-Vis NIR Spectrometer with scan rate 600 nm min^{-1}, photoluminescence (PL) spectra were recorded using Fluorescence Spectrophotometer, F-7000 (Hitachi High-Tech) and decay plot was investigated by Time-correlated single photon counting (TCSPC) system (HORIBA). To study the structural phase and electronic properties of prepared powder sample, Raman spectra were performed using Raman spectroscopy with an excitation wavelength of 532 nm. X-ray powder diffraction (XRD) data was performed in a RIGAKU X-ray diffractometer using Cu Kα radiation ($\lambda = 1.5418$ Å) in the range 10° to 90° to study the crystallinity and structural information. High-resolution transmission electron microscope (HRTEM) was done by using JEOL JEM200 operating at 200 kV.

3. Results and discussion

3.1 *UV–vis spectra of 2D material MoS_2*

In order to investigate the optical property of prepared powder sample, UV–visible absorption spectra were taken at room temperature after dispersing in water, as shown in figure 1. The couple peaks for few-layered 2H-MoS_2 located at 673 and 624 nm in the absorption spectra can be attributed to A and B excitonic interband transition at the K-point of Brillouin zone [15]. The peaks originate due to spin-orbit splitting of valance band at K-point, which is depicted in figure 2c [17]. The C and D excitonic transitions from the deep valance to conduction band edge at M-point of Brillouin zone is the source of absorption peak at 460 and 396 nm in the spectra [21]. All of these features in figure 1 clarify few-layered 2H-MoS_2, as earlier reported for liquid-based exfoliation of monolayer MoS_2 from the bulk [22].

Due to quantum confinement, the bandgap energy increases with decrease in layer number. It can be well explained by using density function theory with generating electronic band structure and density of state (DOS; see figure 2). Here, $a = b = 0.316$ nm and $c = 1.226$ nm were used, which are calculated from XRD and HRTEM result and the calculations with spin–orbit interaction have been carried out using the density functional theory (DFT)-based CASTEP computer program together with the generalized gradient approximation (GGA) with the PBE exchange-correlation function [23]. The plane-wave basis set cut-off was set at 420 eV. The K-point sampling of the Brillouin zone was constructed using Monkhorst-Pack scheme with $9 \times 9 \times 1$ grids in bulk MoS_2. The equilibrium crystal structures were obtained via geometry optimization in the Broyden-Fletcher-Goldfarb-Shanno (BFGS) minimization scheme. In the geometry optimization, criteria of convergence were set to 1.0×10^{-5} eV per atom for energy, 0.03 eV $Å^{-1}$ for force, 1×10^{-3} Å for ionic displacement, and

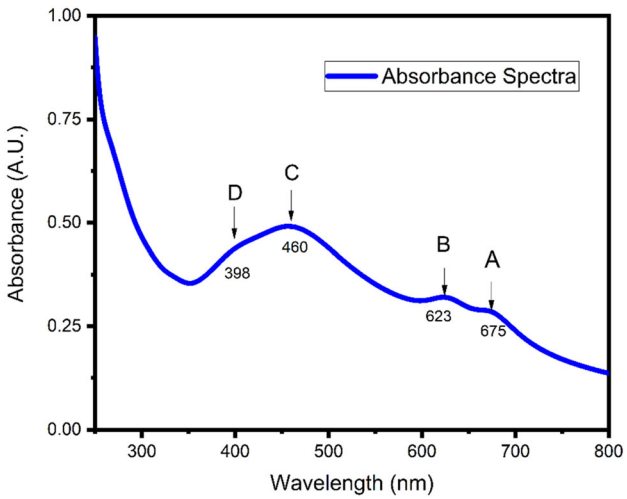

Figure 1. Absorption spectra of MoS_2.

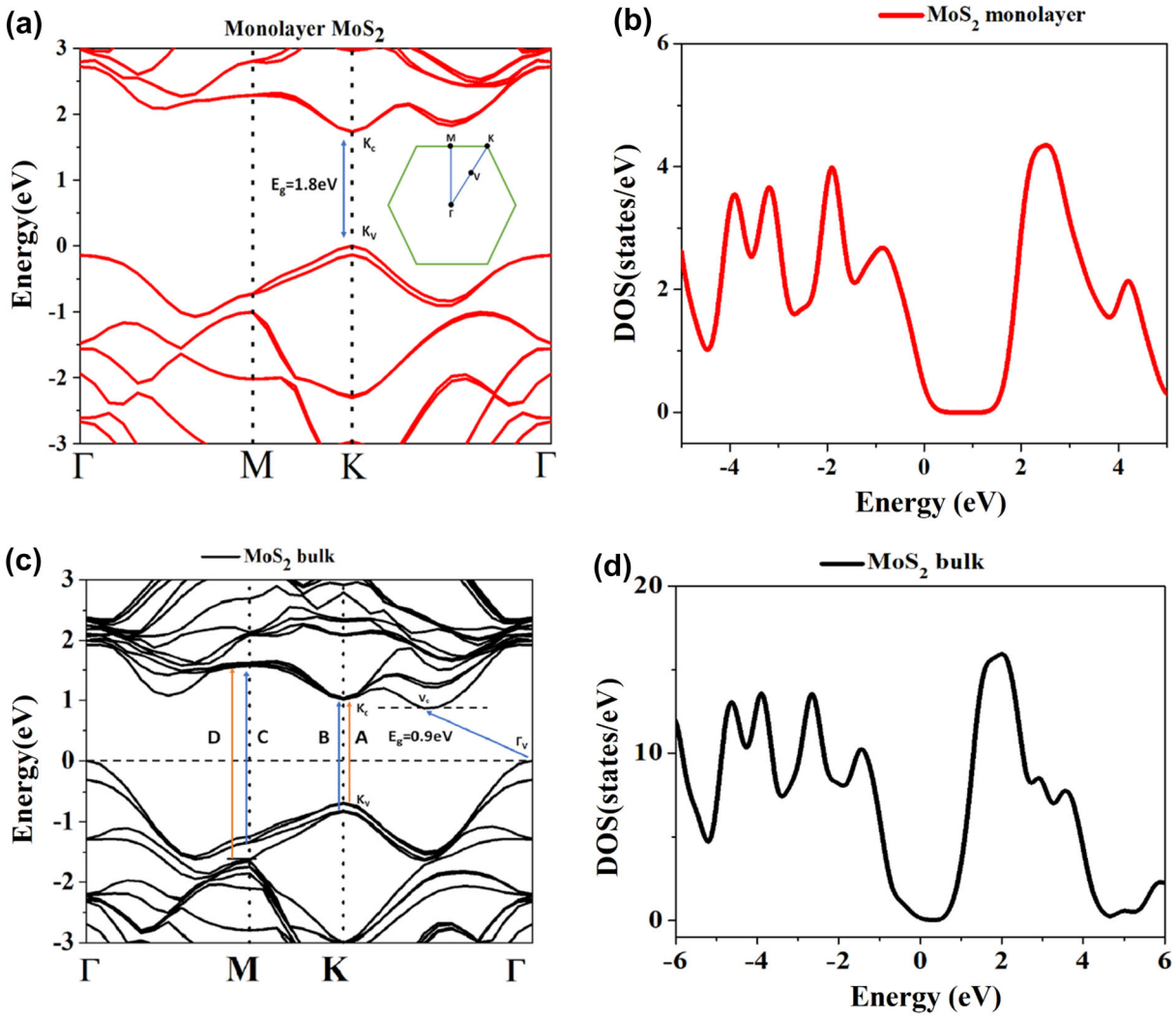

Figure 2. Electronic band structure for (**a**) monolayer MoS_2 and (**c**) bulk MoS_2. Density of state for (**b**) monolayer MoS_2 and (**d**) bulk MoS_2.

0.05 GPa for stress. These parameters are carefully tested and sufficient for a well converged total energy.

According to electronic band structure, the density of states, bandgap energy varies with the number of layers. The bandgaps are 0.9 and 1.8 eV for bulk and monolayer MoS_2, respectively (which is significantly smaller than the experimental value 1.2 eV and 1.9 eV). Yokovkin [24] reported bandgap energy of 0.76 and 1.84 eV for bulk and monolayer MoS_2, respectively, by calculating band structure. In the band structure, few-layered MoS_2 has an indirect transition between Γ_v (valanced band maxima (VBM) and V_c (conduction band minima (CBM)) at almost middle point of Γ and K-point. But monolayer MoS_2 has a direct transition from K_v to K_c point. By decreasing number of layers, band structure of MoS_2 is found to show crucial changes. In the evolution of band structure, K-point remains at the same energy, while Γ point decreases the energy with decreasing layer number [25]. Such outstanding properties of the band structure of MoS_2 is shown due to different components of electronic states at K point and Γ point. At the K point, electronic states are built up with d-orbital of the Mo atom, which has minimum interlayer coupling. Thus, they do not depend on changed layers. While at Γ point, electronic states are composed by a linear combination of d-orbitals of Mo atom and $3P_z$ orbital of S atom. Therefore, the strong coupling between neighbour layers is the main cause of downshift of Γ_v point in its energy level [26–28]. Also due to down shift of Γ_v point, VBM changes from Γ_v to K_v point for monolayer. Thus, $3P_z$ orbitals of S atom plays a crucial role in the transition from indirect to direct bandgap [29]. Valance band maxima shows a large splitting into two bands due to spin–orbit coupling and inversion symmetry in few layers [30].

3.2 *Optical property from UV–vis spectrum*

In this section, optical properties have been calculated and plotted. When a light energy passes through a medium, some of them may be reflected, some transmitted and some absorbed by medium. The intensity of incident light (I_0) must be equal to the intensity of reflected (I_R), transmitted (I_T) and absorbed ray (I_A) [31].

$$I_0 = I_R + I_A + I_T \tag{1}$$

Dividing equation (1) by I_0, we get sum of reflectivity (I_R/I_0), absorptivity (I_A/I_0) and transmissivity (I_T/I_0) equal to one [32].

$$R + A + T = 1 \tag{2}$$

Transmittance can be simulated by using Beer's law $T = 10^{-A}$ [33,34]. The parameter of reflectance can also be calculated by following the equation $R = 1-(A + T)$. The graphical representations of transmittance and reflectance *vs.* wavelength are shown in figure 3c and d. Reflectance are found to be almost constant (0.2 from 300 to 670 nm). Optical absorption coefficient can be calculated by the relation ($\alpha = 2.303 \times A$), where α is the absorption coefficient. The variation of absorption coefficient *vs.* wavelength is presented in figure 3a. This is mirror reflection of absorption spectra. The extinction coefficient (K) of the sample is simulated by using the following relation from experimental data [35].

$$K = \frac{\alpha\lambda}{4\pi t} \tag{3}$$

where λ is the wavelength of electromagnetic wave and t is the sample thickness (t = 1 cm). The variation of K with wavelength (λ) is illustrated in figure 3f. The values of extinction coefficient lie in between 2.0×10^{-6} to 4.0×10^{-6} and it determines the absorption of electromagnetic energy by the material [36]. Its low value indicates that the medium is transparent. The optical refractive index (n) of the medium is also informative and the key parameter to design optical device, which determines the reduction of the speed of light within the medium [32]. The calculation of refractive index (n) is based on reflection and absorption. Thus, expression of refractive index can be represented in terms of reflectance (R) and extinction (K) of the sample [37–40].

$$n = \left[\frac{1+R}{1-R}\right] + \sqrt{\left[\frac{4\times R}{(1-R)^2} - K^2\right]} \tag{4}$$

In figure 3e, the refractive index *vs.* wavelength graph indicates that, the range of n varies from 0.9 to 2.3. The maximum values of r.i (n) are found to be from 300 to 670 nm. The optical conductivity (σ) of the prepared sample is [41]

$$\sigma = \frac{n\alpha c}{4\pi} \tag{5}$$

where c = speed of light (3×10^{10} m s^{-1}). The graphical plot of the optical conductivity *vs.* wavelength is exhibited in figure 3b. The maximum value of optical conductivity is found at 260 nm (5.9×10^9 S cm^{-1}) and it shows wavelength-dependent nature and varies from 1.5×10^9 to 6.0×10^9 S cm^{-1}. The optical refractive index (n) and optical dielectric constants are two important physical parameters utilized for delineating optical properties of the medium. The complex dielectric constant ($\varepsilon_r = \varepsilon_1 + i\varepsilon_2$) is also a measure of light absorbed by the medium. The real part and imaginary part of dielectric constant is directly related to the refractive index and extinction coefficient by the relations [41–43].

$$\varepsilon_1 = n^2 - K^2 \tag{6}$$

$$\varepsilon_2 = 2 \times n \times K \tag{7}$$

When light ray passes through the medium, optical dielectric constant plays an important role since ($n \approx \sqrt{\varepsilon_1}$) [41]. The graphical plot of real part (ε_1) and imaginary part (ε_2) *vs.* wavelength of electromagnetic wave for MoS_2 nanoflakes is pictorial in figure 3g and h. The values of real part and imaginary part of dielectric constant varies from 0.7 to 4.5 and 5.2×10^{-6} to 1.55×10^{-5}, respectively. The maximum value of ε_1 is around 320 and 525 nm while, maximum value of ε_2 is at 470 nm.

In our best knowledge, we take first attempt to calculate dielectric constant as well as refractive index of 2D materials MoS_2 directly from absorption spectrum.

3.3 *PL spectra of 2D material MoS_2*

The PL spectra recorded at room temperature for MoS_2 nanocrystal with excitation wavelength 600 nm is shown in figure 4a. In PL spectra, two prominent peaks are located at 736 and 674 nm due to A and B excitons [44,45]. Emission mechanism for MoS_2 is shown in figure 4b. The broadening peak in the spectra may be due to impurity of the sample. The spin–orbit splitting energy of valance band can be roughly estimated from the peak positions, which is 155 meV. This result tally significantly with the value of 160 meV reported elsewhere for monolayer [46,47]. This splitting energy depends on temperature, because peak position of A and B exciton changes due to temperature. It can be well described by semi-empirical formula based on electron–phonon coupling [49–52]. In this model, exciton energy is

$$E_x^T = E_x^0 - S\langle\hbar\omega\rangle\left[\coth\left(\frac{\langle\hbar\omega\rangle}{K_bT}\right) - 1\right] \tag{8}$$

where K_B is the Boltzmann constant, E_x^0 is the exciton energy at zero temperature, $\langle\hbar\omega\rangle$ refers to the average energy of phonon, which contributes to the temperature change of excitonic energy and S is the dimensionless

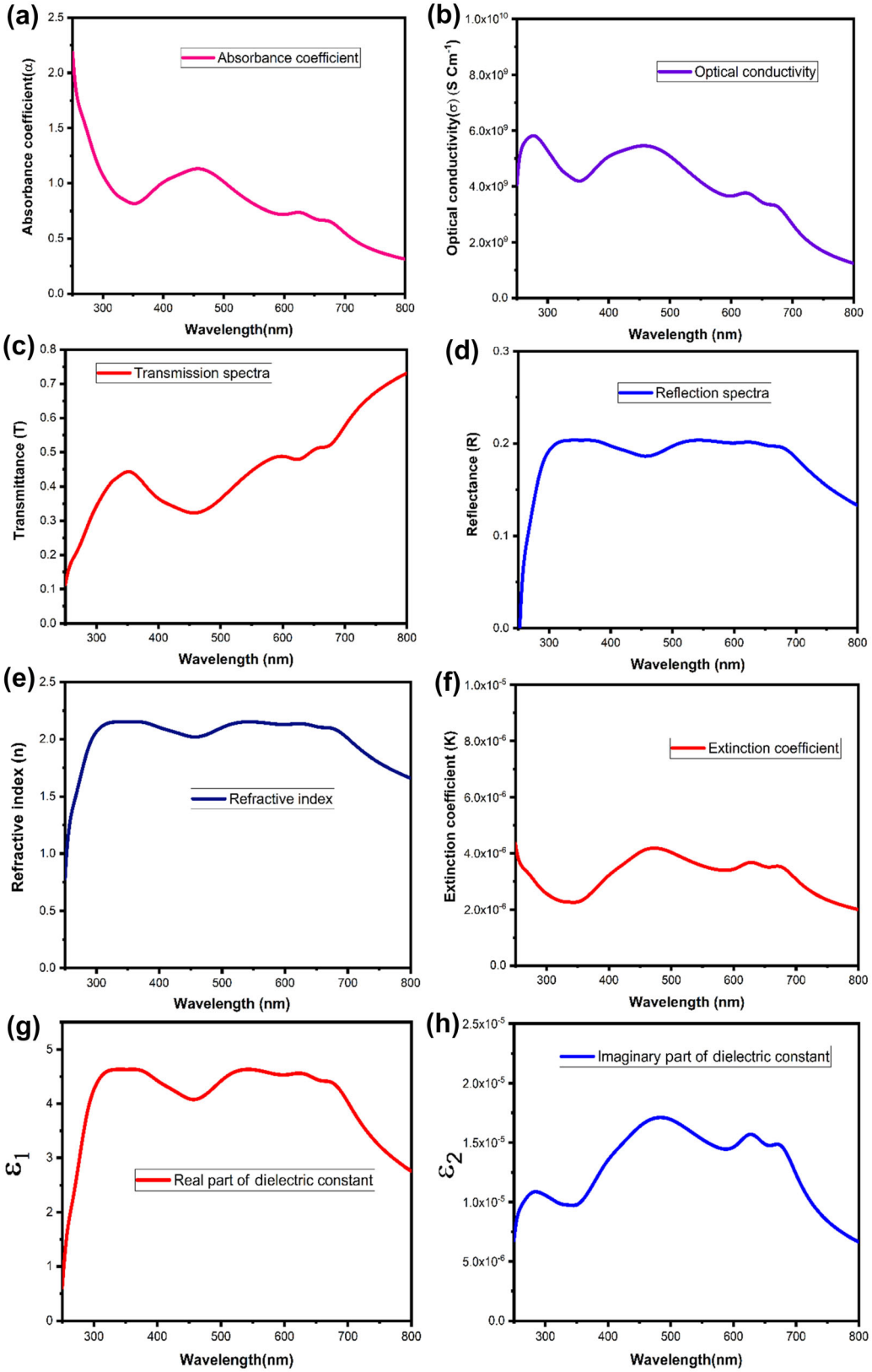

Figure 3. (**a**) Absorption coefficient *vs.* wavelength; (**b**) optical conductivity *vs.* wavelength; (**c**) transmittance *vs.* wavelength; (**d**) reflectance *vs.* wavelength; (**e**) refractive index *vs.* wavelength; (**f**) extinction coefficient *vs.* wavelength; (**g**) real part of dielectric constant *vs.* wavelength and (**h**) imaginary part of dielectric constant *vs.* wavelength graph.

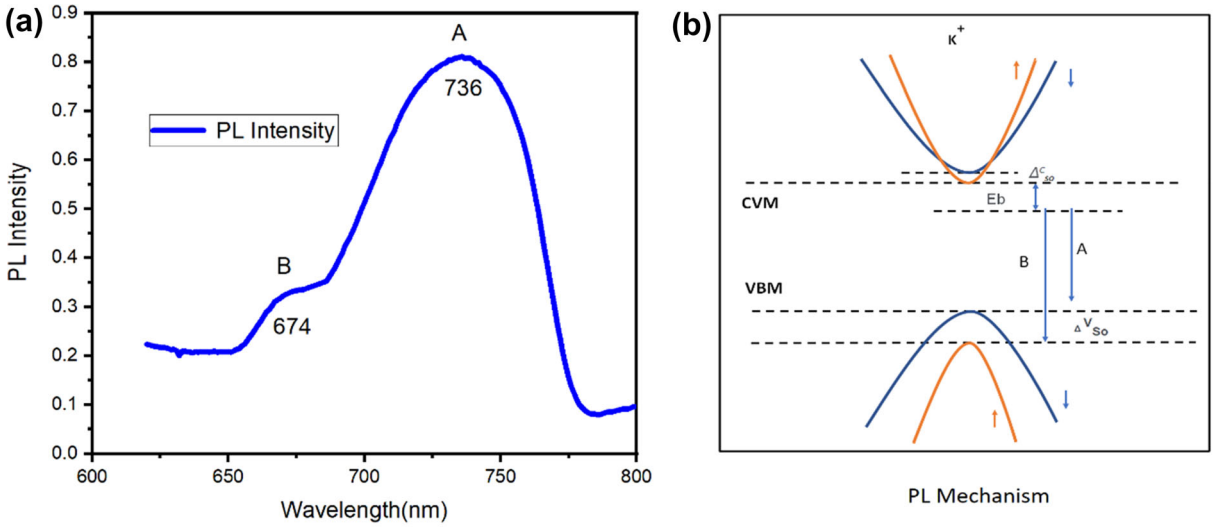

Figure 4. (**a**) PL spectra of MoS_2, and (**b**) PL mechanism.

electron–phonon coupling constant. From equation (8) the temperature-dependent exciton energy (E_x) is simulated (different parameters for A and B exciton are shown in table 1) and has been plotted in figure 5a. This result is in good agreement with experimental results as reported for few-layered MoS_2 [48,52]. Also, it can be predicted that splitting energy is almost constant up to 50 K and then it decreases with increase in temperature, as in figure 5b. At higher temperature, the decrease may be due to thermal expansion, small change in bonding length and increase in photon–phonon interaction [51].

3.4 *TCSPC study*

One of the most excellent experiment time correlated single photons counting (TCSPC) has been investigated for calculating lifetime of the carriers. Here, the sample has been excited at 467 nm using a delta diode laser. The carriers are excited to the higher energy levels and then after certain time they jump to the ground level. The lifetime of carriers is the time measured for the numbers of excited carriers to decay exponentially to 36.8% of the original population. Average lifetime of carriers for MoS_2 sample is found to be 0.75 ns (figure 8a). Ahamed and Neethirajan [53] also determined average lifetime for MoS_2 QD as 0.95 ns].

3.5 *XRD study*

The XRD patterns of as-prepared powder sample are presented in figure 6a. The diffraction peak is obtained at $2\theta = 14.2°$ indicates that MoS_2 layers stack orderly along [002] direction with d-spacing of 0.614 nm, and other diffraction peaks at 28.32, 33.0, 39.43, 58.69 and 69.26 indexed as (004), (101), (103), (105), (110) and (201) plane, respectively. All the diffraction peaks have been perfectly matched with JCPDS data (JCPDS card no- 01-0872416), which assigns as hexagonal crystal structure with lattice parameters $a = b = 0.316$ nm, and $c = 1.226$ nm. No impurity peaks were observed in the XRD pattern. The approximate crystallite size can be roughly estimated by Debye-Scherrer formula [54].

$$D = \frac{K\lambda}{\beta\cos\theta}, \tag{9}$$

where $K = 0.9$, λ is wavelength of X-ray ($\lambda = 1.5404$ Å). β is the full-width at half-maximum (FWHM) in radian and θ is Bragg angle in radian. Few MoS_2 layers are stacked in the c-direction and the calculated average size of MoS_2 in Z-axis is 2.24 nm (along [002] direction). Thus, prepared powder sample has roughly 3 to 4 layers. Guo *et al* [55] also prepared multilayers MoS_2 and calculated 25 layers from XRD data.

Table 1. Values of different parameters for A and B exciton.

	E_x^0 (calculated)	E_x^{293} (experimental)	$\langle\hbar\omega\rangle$ [48]	S [48]
A Exciton	1.752 eV	1.684 eV	23 meV	2.2
B Exciton	1.923 eV	1.840 eV	16 meV	2.3

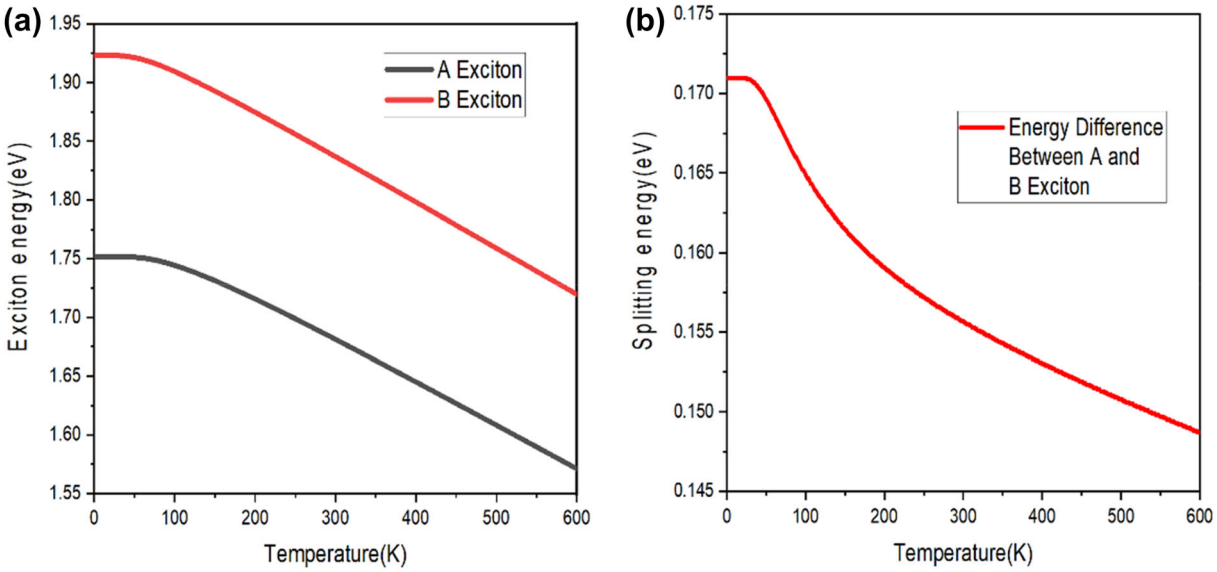

Figure 5. (**a**) Exciton energy *vs.* temperature and (**b**) splitting energy *vs.* temperature graph.

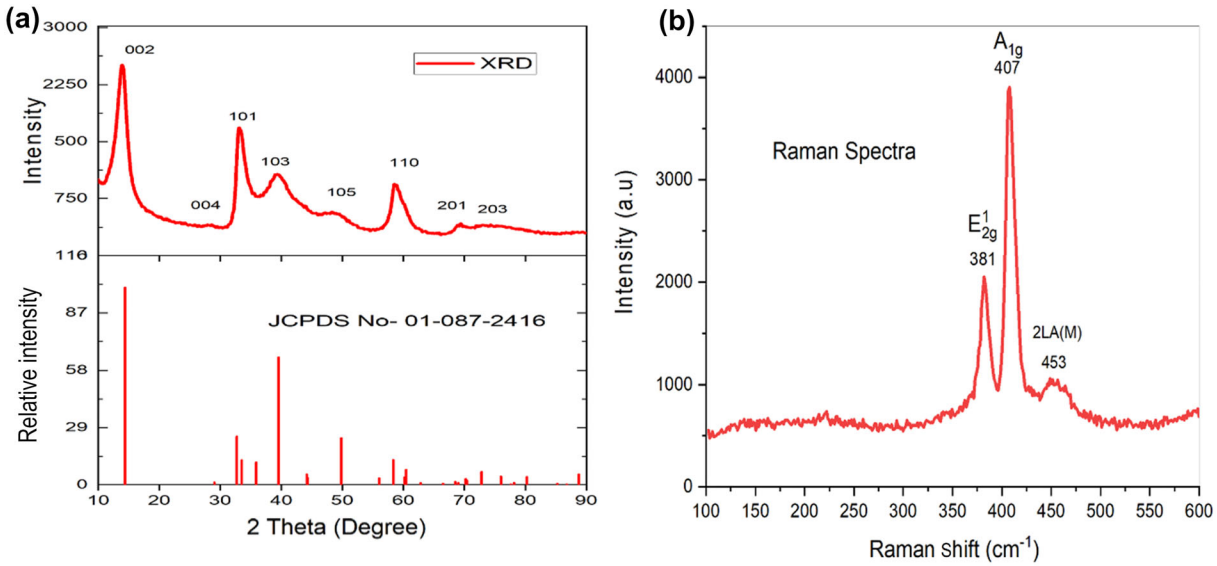

Figure 6. (**a**) XRD pattern of MoS_2 and (**b**) Raman spectra of MoS_2.

3.6 *Raman spectra*

From XRD, it is clear that MoS_2 has hexagonal crystal symmetry and it has P63/mmc space group, and six atoms are contained in its primitive unit cell. Thus, the dispersion relation of 2H-MoS_2 shows 18 branches, among which 15 are optical branches. At the zone centre Γ of the hexagonal Brillouin zone, the irreducible representation of optical phonon modes [25,29] is

$$\begin{aligned}\Gamma_{2H,optical} =& A_{1g}(R) + A_{2u}(IR) + 2B_{2g}(S) + B_{1u}(S) \\ &+ E_{1g}(R) + E_{1u}(IR) \\ &+ 2E_{2g}(R) + E_{2u}(S), \end{aligned} \quad (10)$$

where R, IR, S mean Raman, infrared and silent modes, respectively. The A_{1g}, A_{2u}, B_{2g}, B_{1u} modes demonstrate atomic displacement of out-of-plane and singly degenerate, while the E_{1u}, E_{1g}, E_{2u} and E_{2g} modes exhibit in-plane displacement and are doubly degenerate [56]. A room temperature Raman spectrum of 2H-MoS_2 nanocrystal is illustrated in figure 6b. The location of the two main peaks are 407 cm^{-1} (A_{1g}) and 381 cm^{-1} (E^1_{2g}) in Raman spectra. E_{1g} mode is not noticed because of selection rules. Again, if the filters are not used properly to refuse strong Rayleigh scattering, E^2_{2g} mode cannot be resolved [29]. Another broad peak at 453 cm^{-1} is denoted as 2LA(M), assigned as second-order overtone of longitudinal acoustic phonon at

the M-point of the Brillouin zone. It may be due to 1H-MoS_2 phase [29].

3.7 *Morphology study by HRTEM*

HRTEM results for the exfoliated sample by probe sonicate, as shown in figure 7, indicate that the sample has a nano-sheet structure in irregular shapes. HRTEM is a common and direct method to determine the number of layers microscopically [57]. Here, three-layer nano-sheet are found in the HRTEM, which agrees with XRD result. Fei *et al* [58] also observed that MoS_2 stacks 4–5 layers in vertical direction for low growth temperature. From figure 7c, measured inter-planar spacing 0.58 nm corresponds to (002) plane. Figure 7b manifests that MoS_2 has hexagonal crystal symmetry, which is supported by the XRD result. Also, figure 7d indicates that MoS_2 has a nano-flake structure and average size of nano-flake is 100 nm. Selected area electron diffraction (SAED) are shown in figure 7a. Here, rings appeared due to different crystal planes and these can be indexed using JCPDS data by

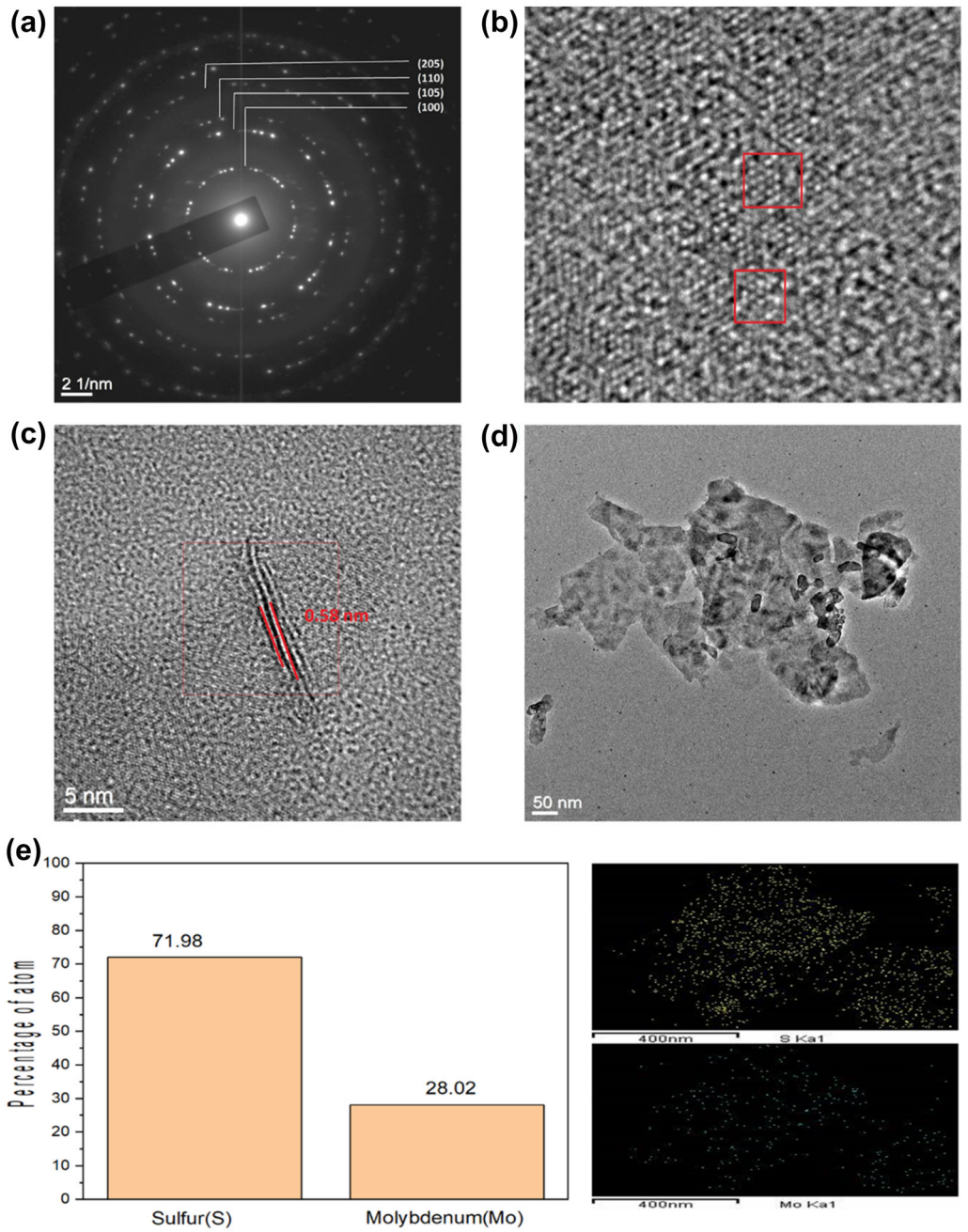

Figure 7. (**a**) SAED of MoS_2; (**b**) hexagonal crystal structure; (**c**) three layers MoS_2; (**d**) nano-flake of MoS_2 and (**e**) composition of molybdenum (Mo) and sulphur (S).

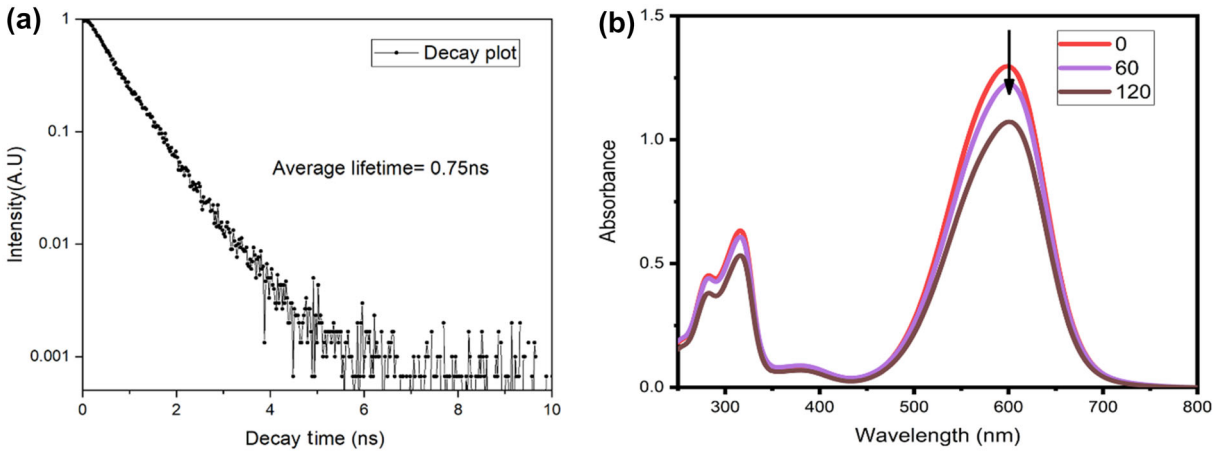

Figure 8. (**a**) Decay plot of MoS_2 and (**b**) MB dye degradation.

ImageJ software. Composition of Mo and S are found from HRTEM result, which is shown in figure 7e by histogram plot.

4. Photocatalytic activity

In order to investigate the photocatalytic performance of prepared sample, UV-Vis-NIR spectrometer has been used. At first, dye solution (2 mg in 50 ml) and the nanomaterial solution (3 mg in 10 ml) have been prepared with distilled water. Then, two solutions were mixed under dark condition and kept for 30 min without irradiation in order to obtain equilibrium of dye adsorption. After that, the solution was irradiated under the light (approximate light intensity 0.75 Wm^{-2}). After light is ON, absorption spectra are recorded under 60-min time interval, which is shown in figure 8b. Down-shift of peak position clearly indicates that MB dye has been degraded.

5. Conclusion

In summary, crystalline 2H-MoS_2 has been synthesized by hydrothermal method. To investigate optical and structural properties, absorption spectra, PL spectra, TCSPC, XRD, Raman and HRTEM have been performed and explained with appropriate mechanism. Dielectric constant as well as refractive index is calculated from experimental data. Simulated splitting energy of valance band are dependent on temperature. The calculated excitonic energy agrees well with the available electron–phonon coupling theory. Exfoliated MoS_2 has three-layers, which is suitable for different applications. For photocatalytic activity of MB dye degradation, activity depends directly on concentration of nanomaterials.

References

[1] Afzaal M and O'Brien P 2006 *J. Mater. Chem.* **16** 1597
[2] Fan P, Chettiar U K, Cao L, Afshinmanesh F, Engheta N and Brongersma M L 2012 *Nat. Photon.* **6** 380
[3] Hernández-Ramírez A and Medina-Ramírez I 2015 (eds) *Photocatalytic semiconductors* (Switzerland: Springer)
[4] Karthikeyan C, Arunachalam P, Ramachandran K, Al-Mayouf A M and Karuppuchamy S 2020 *J. Alloys Compd.* **828** 154281
[5] Khan I, Saeed K and Khan I 2019 *Arab. J. Chem.* **12** 908
[6] Krasnok A, Lepeshov S and Alú A 2018 *Opt. Express* **26** 15972
[7] Berkelbach T C, Hybertsen M S and Reichman D R 2013 *Phys. Rev. B* **88** 045318
[8] Rasmussen F A and Thygesen K S 2015 *J. Phys. Chem. C* **119** 13169
[9] Portone A, Romano L, Fasano V, Di Corato R, Camposeo A, Fabbri F *et al* 2018 *Nanoscale* **10** 21748
[10] Goh E S, Chen T P, Sun C Q and Liu Y C 2010 *J. Appl. Phys.* **107** 024305
[11] Dupont C, Lemeur R, Daudin A and Raybaud P 2011 *A Dft Study J. Catal.* **279** 276
[12] Muratore C, Varshney V, Gengler J J, Hu J J, Bultman J E, Smith T *et al* 2013 *Appl. Phys. Lett.* **102** 081604
[13] Singh N, Jabbour G and Schwingenschlgl U 2012 *Eur. Phys. J. B* **85** 392
[14] Wang X, Zhang Z, Chen Y, Qu Y, Lai Y and Li J 2014 *J. Alloys Compd.* **600** 84
[15] Ahmad R, Srivastava R, Yadav S, Singh D, Gupta G and Chand S 2017 *J. Phys. Chem. Lett.* **8** 1729
[16] Feng C, Ma J, Li H, Zeng R, Guo Z and Liu H 2009 *Mater. Res. Bull.* **44** 1811
[17] Saha N, Sarkar A, Ghosh A B, Dutta A K, Bhadu G R, Paul P *et al* 2015 *RSC Adv.* **5** 88848
[18] Luo L, Shi M, Zhao S, Tan W, Lin X and Wang H 2019 *J. Saudi Chem. Soc.* **23** 762
[19] Li Y, Xiang F, Lou W and Zhang X 2019 *IOP Conf. Ser. Earth Environ. Sci.* **300** 052021
[20] Mehrjouei M, Müller S and Möller D 2014 *J. Clean. Prod.* **65** 178

[21] Wang J, Zhang W, Wang Y, Zhu W, Zhang D and Li Z 2016 *Part. Part. Syst. Charact.* **33** 825
[22] Magda G Z, Pető J, Dobrik G, Hwang C, Biró L P and Tapasztó L 2015 *Sci. Rep.* **5** 1
[23] Clark S J, Segall M D, Pickard C J, Hasnip P J, Probert M I, Refson K *et al* 2005 *Z. Kristallogr. Cryst. Mater.* **220** 567
[24] Yakovkin I N 2016 *Crystals* **6** 143
[25] Sun L 2016 Article ID:100855320. dhttps://doi.org/10.32657/10356/66936
[26] Kuc A, Zibouche N and Heine T 2011 *Phys. Rev. B* **83** 245213
[27] Song I, Park C and Choi H C 2015 *RSC Adv.* **5** 7495
[28] Alidoust N, Bian G, Xu S Y, Sankar R, Neupane M, Liu C *et al* 2014 *Nat. Commun.* **5** 1
[29] Samadi M, Sarikhani N, Zirak M, Zhang H, Zhang H L and Moshfegh A Z 2018 *Nanoscale Horiz.* **3** 90
[30] Yu H, Cui X, Xu X and Yao W 2015 *Natl. Sci. Rev.* **2** 57
[31] Trnjanin N 2019 MS thesis (Chalmers University of Technology)
[32] Abdullah R M, Aziz S B, Mamand S M, Hassan A Q, Hussein S A and Kadir M F Z 2019 *Nanomaterials* **9** 874
[33] Brza M A, Aziz S B, Anuar H and Al Hazza M H F 2019 *Int. J. Mol. Sci.* **20** 3910
[34] Aziz S B, Rasheed M A, Hussein A M and Ahmed H M 2017 *Mater. Sci. Semiconduct. Process* **71** 197
[35] Aziz S B, Hussein S, Hussein A M and Saeed S R 2013 *Int. J. Met.* Article ID 123657 doi:https://doi.org/10.1155/2013/123657
[36] Kittel C and McEuen P 2018 (eds) *Introduction to solid state physics* (Singapore: John Wiley & Sons)
[37] Becerril H A, Mao J, Liu Z, Stoltenberg R M, Bao Z and Chen Y 2008 *ACS Nano* **2** 463
[38] Ghosh T N, Bhunia A K, Pradhan S S and Sarkar S K 2020 *J. Mater. Sci.: Mater. Electron.* **31** 15919
[39] Abdelhamied M M, Atta A, Abdelreheem A M, Farag A T M and El Okr M M 2020 *J. Mater. Sci.: Mater. Electron.* **31** 22629
[40] Soylu M, Al-Ghamdi A A and Yakuphanoglu F 2015 *J. Phys. Chem.* **85** 26
[41] Bhunia A K and Saha S 2021 *J. Mater. Sci.: Mater. Electron.* **32** 9912
[42] Aziz S B 2017 *Nanomaterials* **7** 444
[43] Aziz S B, Abdullah O G, Hussein A M, Abdulwahid R T, Rasheed M A, Ahmed H M *et al* 2017 *J. Mater. Sci. Mater. Electron.* **28** 7473
[44] Wei X, Yu Z, Hu F, Cheng Y, Yu L, Wang X *et al* 2014 *AIP Adv.* **4** 123004
[45] Chen F, Wang L, Wang T and Ji X 2017 *Opt. Mater. Express* **7** 1365
[46] Mak K F, Lee C, Hone J, Shan J and Heinz T F 2010 *Phys. Rev. Lett.* **105** 136805
[47] Eda G, Yamaguchi H, Voiry D, Fujita T, Chen M and Chhowalla M 2011 *Nano Lett.* **11** 5111
[48] Christopher J W, Goldberg B B and Swan A K 2017 *Sci. Rep.* **7** 1
[49] Karmakar S, Biswas S and Kumbhakar P 2018 *Appl. Surf. Sci.* **455** 379
[50] Rassay S S 2017 PhD thesis (New Jersey Institute of Technology)
[51] Golovynskyi S, Irfan I, Bosi M, Seravalli L, Datsenko O I, Golovynska I *et al* 2020 *Appl. Surf. Sci.* **515** 146033
[52] Helmrich S 2020 (eds) *Optical properties of quasiparticles in monolayer and bilayer TMDCs* Technische Universitaet Berlin (Germany)
[53] Ahmed S R and Neethirajan S 2018 *Global Challenges* **2** 1700071
[54] Rana C, Bera S R and Saha S 2021 *J. Electron. Mater.* **50** 1177
[55] Guo X, Wang Z, Zhu W and Yang H 2017 *RSC Adv.* **7** 9009
[56] Zhang X, Qiao X F, Shi W, Wu J B, Jiang D S and Tan P H 2015 *Chem. Soc. Rev.* **44** 2757
[57] Gao D, Si M, Li J, Zhang J, Zhang Z, Yang Z, Xue D *et al* 2013 *Nanoscale Res. Lett.* **8** 1
[58] Fei L, Lei S, Zhang W B, Lu W, Lin Z, Lam C H *et al* 2016 *Nat. Commun.* **7** 1